Supporting Information

Shifting the scaling relations of single-atom catalysts for facile methane activation by tuning the coordination number

Changhyeok Choi,[a] Sungho Yoon,[b] and Yousung Jung*[a]

[a]*Department of Chemical and Biomolecular Engineering, Korea Advanced Institute of Science and Technology (KAIST), 291 Daehak-ro, Yuseong-gu, Daejeon 34141, Republic of Korea.*

[b]*Department of Chemistry, Chung-Ang University, Dongjak-Gu, Seoul 06974, Republic of Korea*

Calculation details for zeolites and $IrO_2(110)$

We considered $[CuO]^+$ and $[Cu\text{-}O\text{-}Cu]^{2+}$ cations embedded zeolites. The CHA and MOR framework were used to construct $[CuO]^+$ (CHA/Cu-O) and $[Cu\text{-}O\text{-}Cu]^{2+}$ (MOR/Cu-O-Cu), respectively. For both catalysts, 8MR channel was considered. We used stable structures of CHA/Cu-O[1] and MOR/Cu-O-Cu[2] which have been previously revealed in the literatures (**Figure S1**). For IrO_2, a rutile (110) facet was used. A (2 x 2) supercell with 4 layers, while bottom two layers were fixed to their optimized bulk positions. We considered O adsorbed at CUS as an active site (**Figure S2**). For zeolites, the gamma point was used while a (4 x 4 x 1) k-point sampling was employed for $IrO_2(110)$.[3]

Reaction rate for methane activation

We obtain the overall reaction rate for methane activation by using E_f and E_H as suggested by Nørskov and coworkers.[4]

$$rate = \vartheta_{motif}\frac{k_B T}{h}exp\left(\frac{-\Delta G_a}{k_B T}\right)$$

$$\vartheta_{motif} = \frac{\sqrt{P_{O_2}}exp\left(\frac{-G_f}{k_B T}\right)}{1+\sqrt{P_{O_2}}exp\left(\frac{-G_f}{k_B T}\right)}$$

The ϑ_{motif} is the fraction of available *O atoms for methane activation and the remaining terms represent the rate of methane activation at *O atoms. Here, we consider P_{O_2}= 1 bar and T = 150 °C to simulate the low temperature methane activation. The ΔG_a represents activation free energy of C-H bond cleavage of methane at active *O atom (*O + CH_4(g) → *OH + ·CH_3(g)),

which is predicted by using the universal scaling relationship between E_a and E_H as below.[4, 5]

$$E_a = 0.75\ E_H + 1.96\ (eV)$$

Consequently, we obtain a 2D-volcano plot of rate for methane activation by using the two descriptors (G_f and G_H).

Fractional degree of charge delocalization

To estimate the ability of charge delocalization of catalysts upon *O formation, we compare the fractional degree of charge delocalization (χ_{ox}) as suggested by Snurr and coworkers.[5]

$$\chi_{ox} = 1 - \frac{\Delta q_M}{|q_O|}$$

Δq_M is the change in partial charge of metal atom following the *O formation and q_O is the partial charge on the *O. To maintain the charge neutrality, $|q_O|$ equals to the sum of Δq_M and change in charge of framework atoms (Δq_{frame}, all atoms except for metal and *O). The $\chi_{ox} = 0$ implies that *O formation occurs without any charge delocalization ($\Delta q_M = |q_O|$), while the $\chi_{ox} = 1$ implies fully delocalized ($\Delta q_M = 0$). The atomic charges are obtained by the Bader charge analysis.[6]

A wide range of χ_{ox} values are obtained at each moiety, however, the relationship between χ_{ox} and different scaling line was not observed. For example, the χ_{ox} values of M@C_4 range almost evenly from 0.1 (poorly delocalized) to 0.9 (well delocalized) (***Figure S4*c**). However, all M@C_4 catalysts fall on the same scaling line, different from the scaling line of M@C_2 or M@C_3 (**Figure S4d**).

Formation energy of M@N_xC_y catalysts

The formation energy of M@N_xC_y catalysts (E_{form}) is obtained by the equation,

$$E_{form} = E(M@N_xC_y) - E(\text{graphene}) + l\mu(C) - m\mu(N) - \mu(M).$$

Here, l and m represent the number of carbon defects and nitrogen in the slab model, E is the electronic total energy, and μ(C), μ(N) and μ(M) are the chemical potential of carbon, nitrogen and metal defined as the electronic total energy per atom in pristine graphene, N_2(g) and bulk metals (unit cell), respectively.

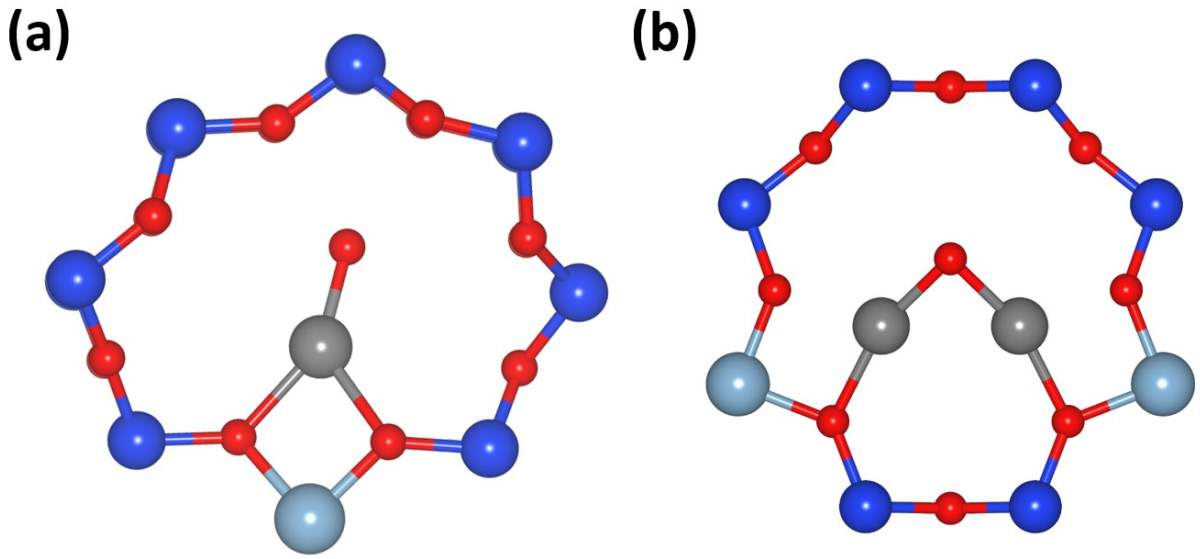

Figure S1. The optimized structures of (a) CHA/Cu-O and (b) MOR/Cu-O-Cu. Grey, sky blue, blue and red balls represent Cu, Al, Si and O atoms, respectively.

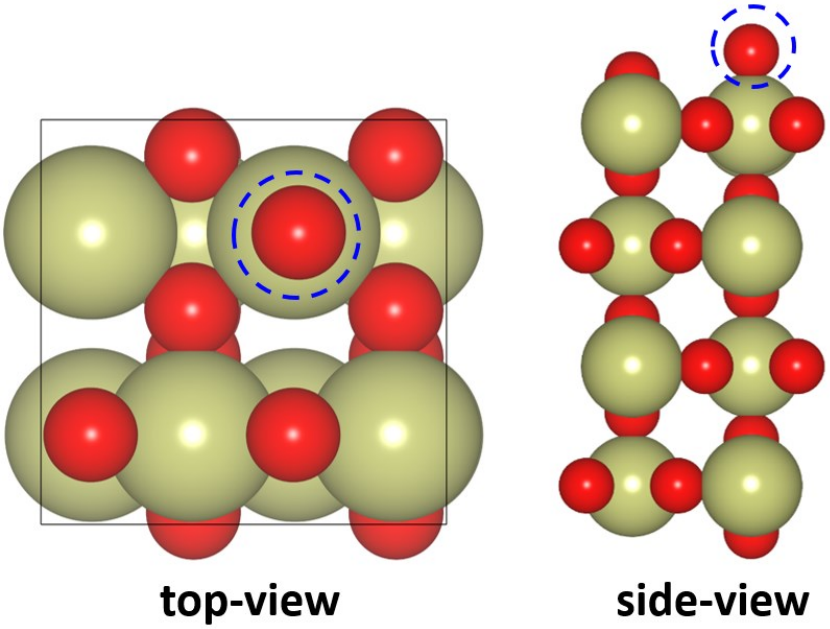

Figure S2. The optimized geometry for *O on CUS in IrO_2(110). Yellow and red balls represent Ir and O atoms, respectively. The reactive *O is highlighted in blue circle.

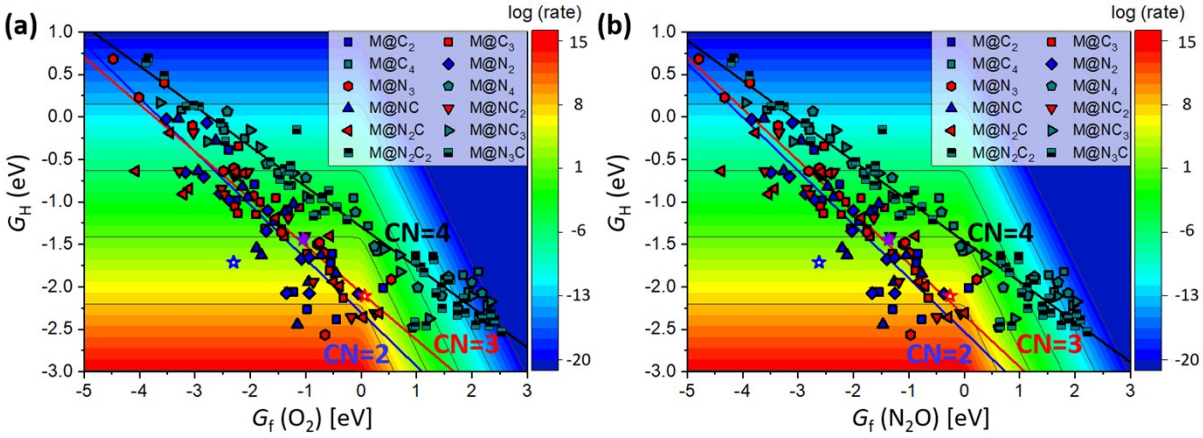

Figure S3. 2D-volcano plot for methane activation at 150 °C as a function of G_f and G_H obtained by using (a) O_2 and (b) N_2O as an oxidant. When using N_2O, G_f is obtained via the reaction of * + N_2O(g) → *O + N_2(g). Blue, red and black lines represent linear scaling lines of CN = 2, 3 and 4, respectively.

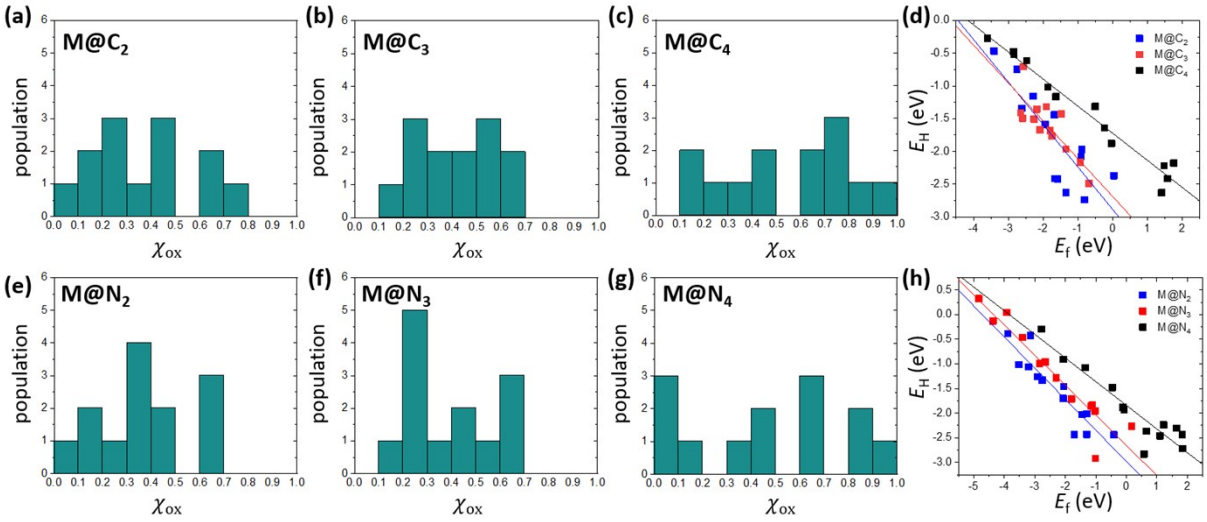

Figure S4. Distribution of χ_{ox} in (a) M@C_2, (b) M@C_3, (c) M@C_4, (e) M@N_2, (f) M@N_3 and (g) M@N_4. Scaling relationship between E_f vs. E_H on (d) M@C_x and (h) M@N_x. Blue, red and black represent CN = 2, 3 and 4, respectively.

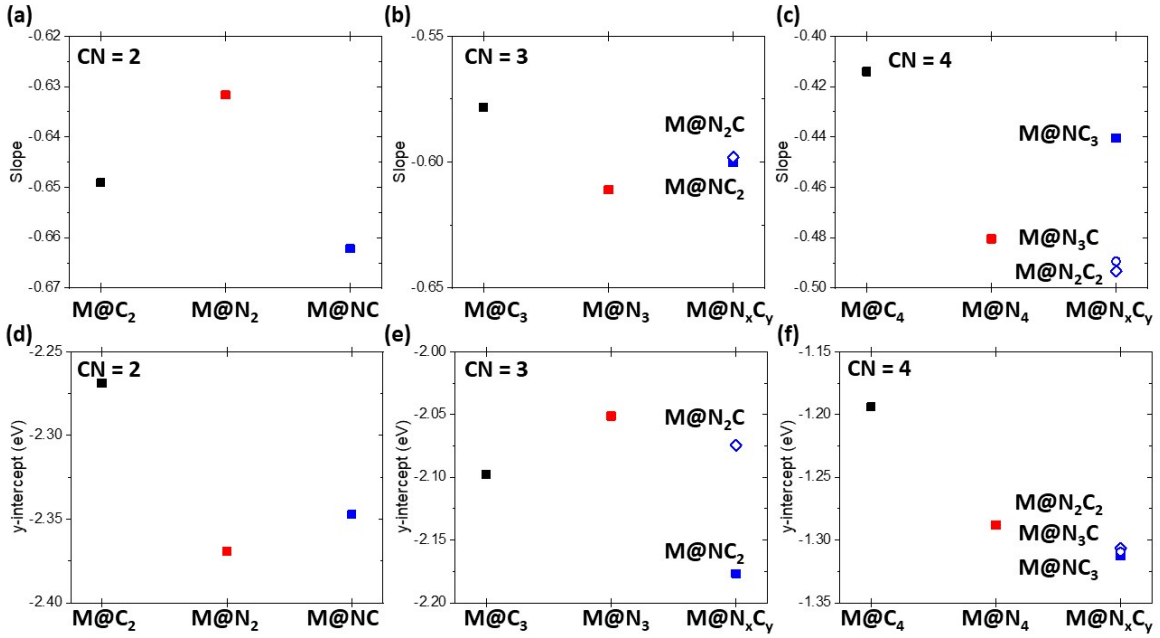

Figure S5. Change of slope by ligand atom when (a) CN = 2, (b) CN = 3 and (c) CN = 4. Change of y-intercept by ligand atom when (d) CN = 2, (e) CN = 3 and (f) CN = 4. Black, red and blue represent M@C_x, M@N_x and M@N_xC_y, respectively.

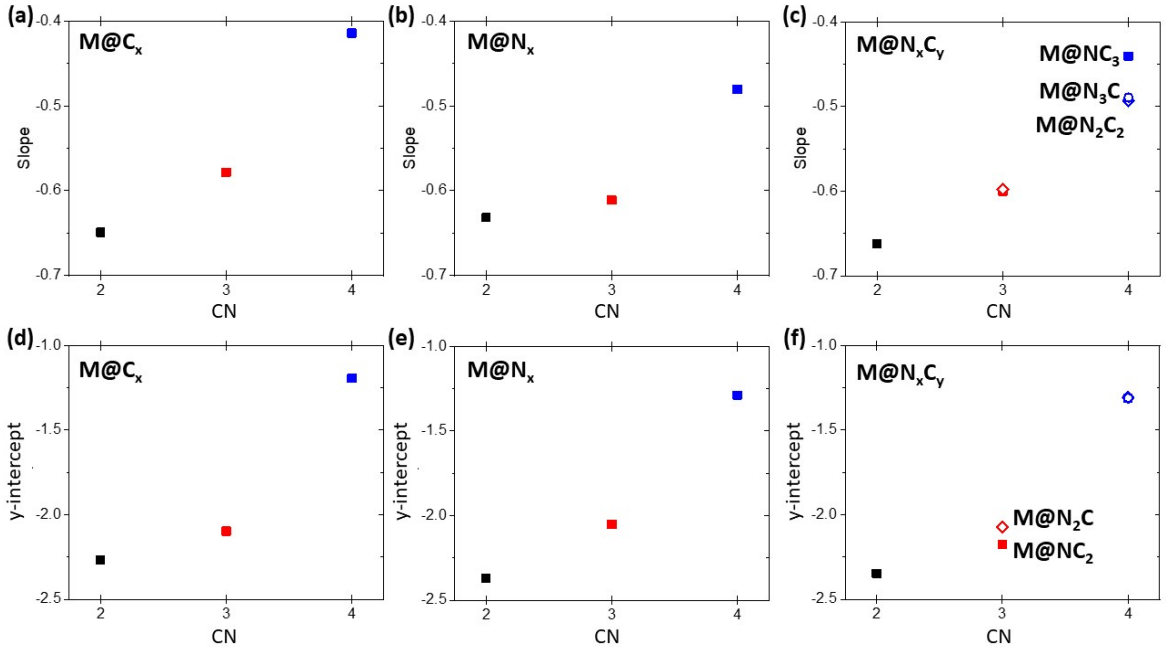

Figure S6. Change of slope by CN on (a) M@C_x, (b) M@N_x and (c) M@N_xC_y. Change of y-intercept by CN on (d) M@C_x, (e) M@N_x and (f) M@N_xC_y. Black, red and blue represent CN = 2, 3 and 4, respectively.

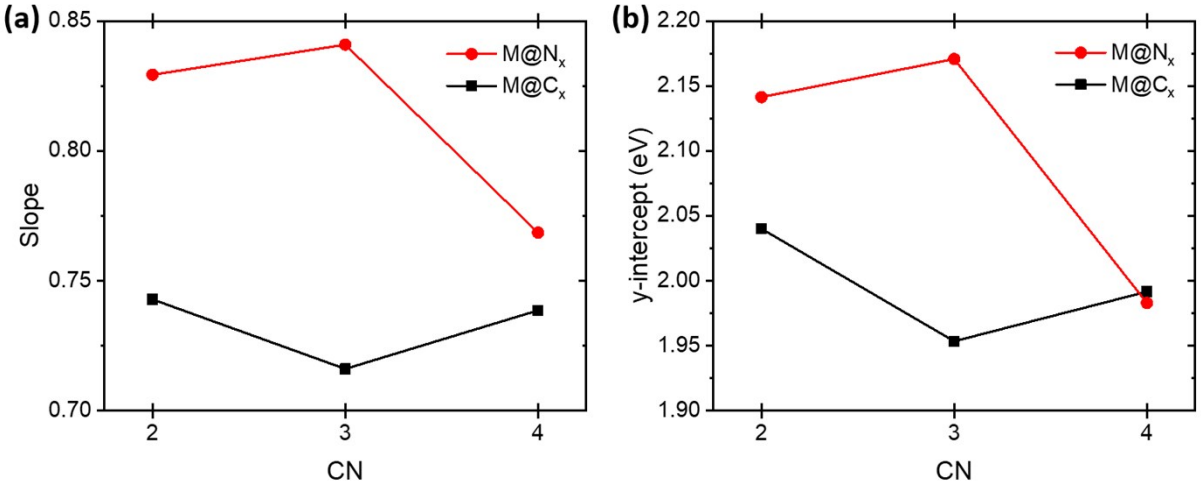

Figure S7. Slope and y-intercept of linear scaling line between E_H and $E_a(CH_4)$.

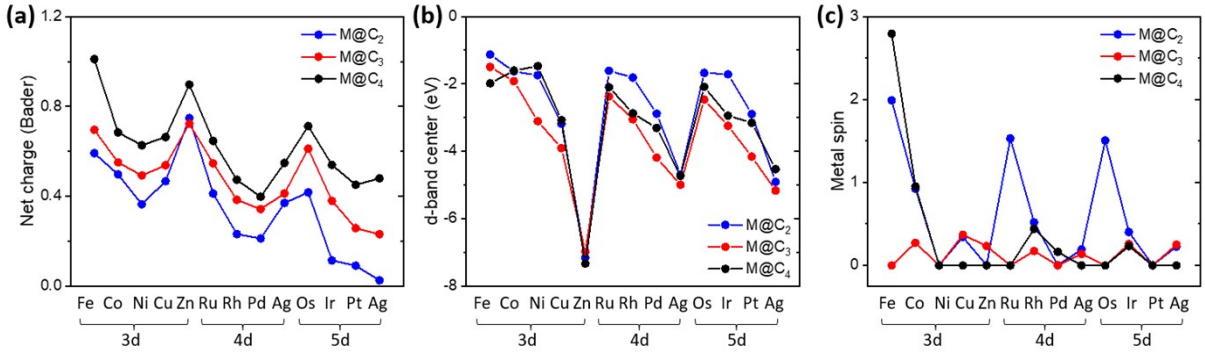

Figure S8. Changes of (a) net charge obtained by the Bader charge analysis, (b) d-band center and (c) spin momentum of metal in M@C_x catalysts with CN. Blue, red and black represent M@C_2, M@C_3 and M@C_4, respectively.

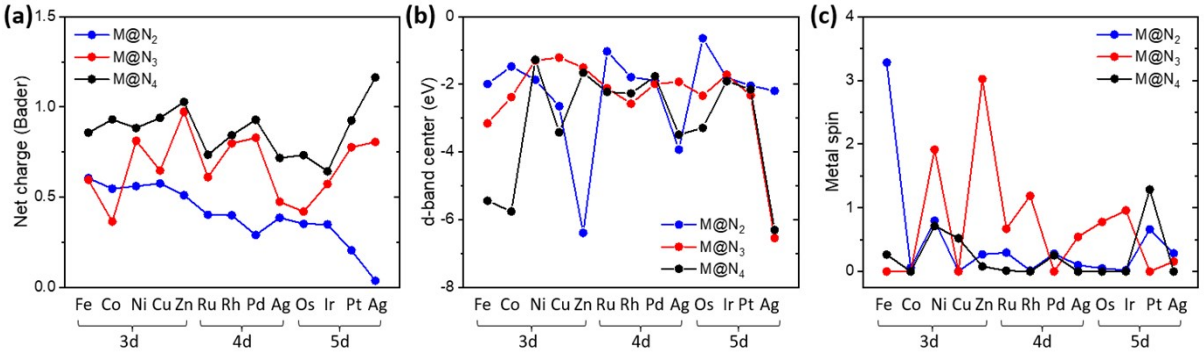

Figure S9. Changes of (a) net charge obtained by the Bader charge analysis, (b) d-band center and (c) spin momentum of metal in M@N_x catalysts with CN. Blue, red and black represent M@N_2, M@N_3 and M@N_4, respectively.

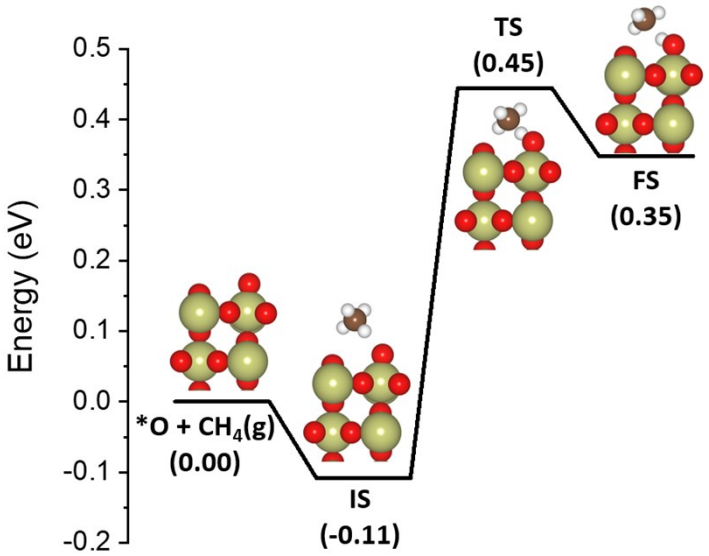

Figure S10. Free energy diagram for methane activation on $IrO_2(110)$. The $CH_4(g)$ and bottom two layers are omitted for the clarity. All energies are in eV.

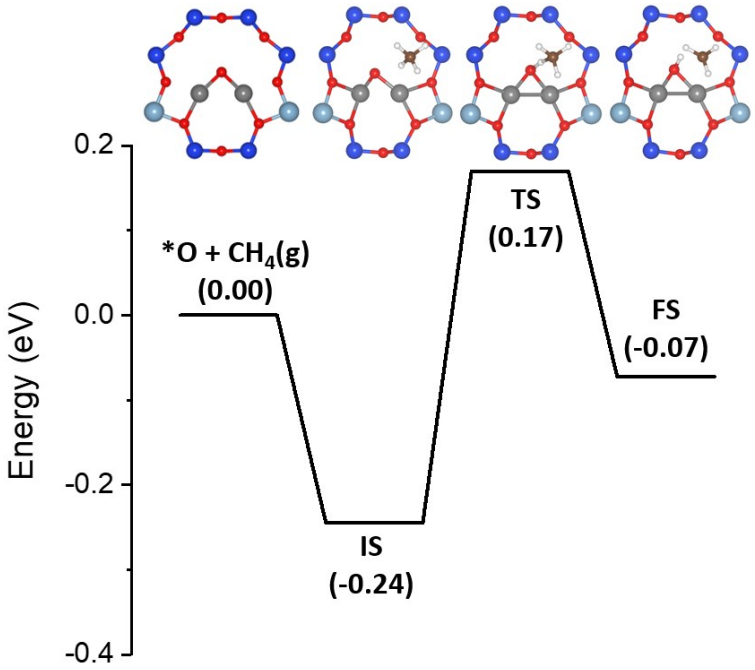

Figure S11. Free energy diagram for methane activation on MOR/Cu-O-Cu. All energies are in eV.

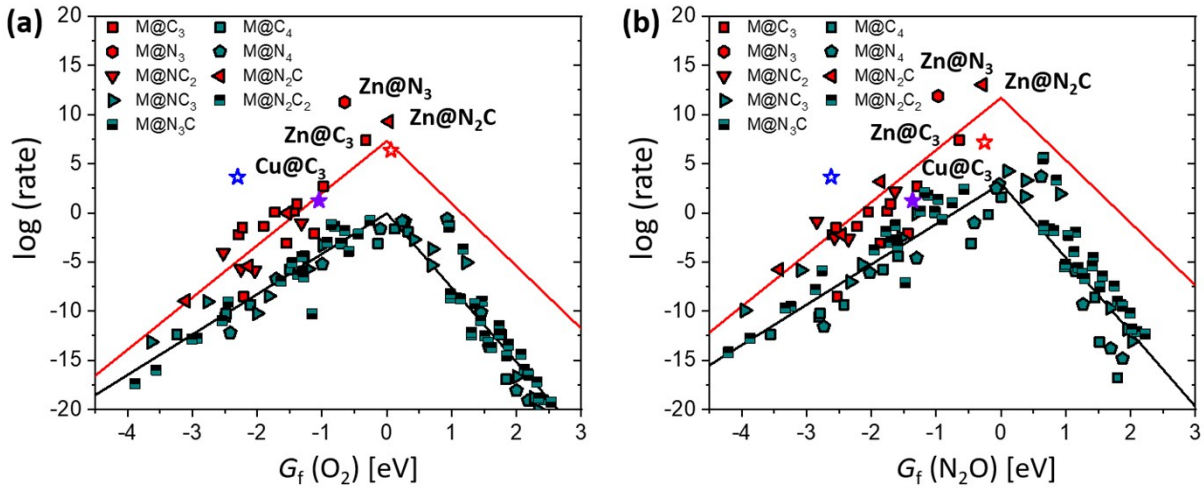

Figure S12. 1D-volcano plot for methane activation on stable $M@N_xC_y$ catalysts obtained by using (a) O_2 and (b) N_2O as an oxidant. Red and black lines represent scaling line in CN = 3 and CN = 4, respectively

Table S1. Calculated $E_a(CH_4)$ on $M@N_x$ and $M@C_x$ catalysts in eV.

metal	$M@N_2$	$M@N_3$	$M@N_4$	$M@C_2$	$M@C_3$	$M@C_4$
Ag	0.15	0.27	0.17		0.46	0.31
Au		0.61	-0.13	0.23		
Co	1.02	1.03	0.47	0.78	0.78	1.10
Cu	0.43	0.49	0.13	0.09	0.57	0.36
Fe	1.33		1.18	1.24	0.83	
Ir			0.85		1.02	
Ni	0.68	0.62	0.31	0.45	0.98	0.75
Os					0.83	
Pd	0.51	0.60	0.03	0.25	0.91	0.61
Pt	1.13		0.16	0.58		1.06
Rh	0.88	1.50		0.84	0.84	
Ru					0.64	
Zn	0.12	-0.22	-0.13	0.35	0.12	-0.04

Table S2. Binding energy of single metal atom (E_b) at @C_x and @N_x defective sites relative to the bulk states (eV)

Metal	@C_2	@C_3	@C_4	@N_2	@N_3	@N_4
Fe	1.39	-2.42	-1.06	3.06	0.55	-2.27
Co	1.31	-2.52	-1.00	2.70	0.52	-2.34
Ni	0.48	-1.95	-1.33	2.20	0.62	-2.62
Cu	1.62	0.09	-1.29	2.21	0.77	-1.17
Zn	1.68	0.06	-1.35	1.57	-0.16	-2.15
Ru	2.61	-1.98	-0.90	4.16	2.10	-0.06
Rh	1.51	-2.34	-0.88	3.03	2.04	-1.29
Pd	0.46	-1.45	-0.54	2.73	1.79	-1.73
Ag	2.11	1.00	0.15	2.33	1.11	0.69
Os	3.86	-1.01	-0.41	5.65	3.77	0.85
Ir	2.28	-1.73	-0.78	4.46	3.73	-0.71
Pt	0.61	-1.49	-1.34	3.81	3.16	-1.80
Au	1.93	0.81	-1.12	3.02	2.23	0.22

Table S3. Binding energy of single metal atom (E_b) at @N_xC_y defective sites relative to the bulk states (eV)

Metal	@NC	@NC_2	@N_2C	@NC_3	@$N_2C_{2(1)}$	@$N_2C_{2(2)}$	@$N_2C_{2(3)}$	@N_3C
Fe	1.71	-0.65	-0.29	-2.32	-2.20	-3.05	-2.77	-2.60
Co	1.24	-0.59	-0.37	-2.26	-2.24	-3.06	-2.79	-2.73
Ni	1.12	-0.20	0.10	-2.85	-3.01	-3.77	-3.42	-3.27
Cu	0.99	0.84	0.53	-2.66	-2.26	-3.08	-2.67	-2.00
Zn	0.68	0.53	-0.55	-1.98	-1.43	-2.34	-2.53	-2.14
Ru	2.78	0.22	0.69	-1.37	-0.40	-1.24	-1.56	-0.51
Rh	1.36	-0.17	0.65	-1.80	-2.36	-1.99	-2.06	-1.60
Pd	1.21	0.60	0.56	-1.85	-2.05	-2.82	-2.42	-2.36
Ag	1.94	1.56	1.18	-1.24	-0.86	-1.74	-1.31	-0.67
Os	4.11	1.35	2.16	-0.76	0.33	-0.58	-0.79	0.28
Ir	2.50	0.72	1.85	-1.62	-0.86	-1.82	-1.76	-1.20
Pt	1.71	1.02	1.49	-2.43	-2.36	-3.20	-2.71	-2.51
Au	1.94	1.71	1.38	-2.29	-1.70	-2.67	-2.18	-1.44

Table S4. E_{form} of promising $M@N_xC_y$ catalysts and experimentally synthesized $M@N_xC_y$ catalysts. Asterisk (*) denotes experimentally reported $M@N_xC_y$ catalysts.

Catalysts	E_{form} (eV)
$Cu@C_3$	8.12
$Zn@C_3$	8.09
$Zn@N_2C$	4.28
$Zn@N_3$	3.18
$*Ag@N_4$	4.40
$*Ru@N_4$	3.65
$*Co@N_4$	1.36
$*Cu@N_4$	2.53

References

1. A. R. Kulkarni, Z.-J. Zhao, S. Siahrostami, J. K. Nørskov and F. Studt, *ACS Catal.*, 2016, **6**, 6531-6536.
2. M. H. Mahyuddin, T. Tanaka, Y. Shiota, A. Staykov and K. Yoshizawa, *ACS Catal.*, 2018, **8**, 1500-1509.
3. H. J. Monkhorst and J. D. Pack, *Phys. Rev. B*, 1976, **13**, 5188-5192.
4. A. A. Latimer, A. R. Kulkarni, H. Aljama, J. H. Montoya, J. S. Yoo, C. Tsai, F. Abild-Pedersen, F. Studt and J. K. Nørskov, *Nat. Mater.*, 2017, **16**, 225-229.
5. A. S. Rosen, J. M. Notestein and R. Q. Snurr, *ACS Catal.*, 2019, **9**, 3576-3587.
6. W. Tang, E. Sanville and G. Henkelman, *J. Phys.: Condens. Matter*, 2009, **21**, 084204.